Published online 23 November 2010 *Nucleic Acids Research, 2011, Vol. 39, No. 7* **2931–2942**
doi:10.1093/nar/gkq1177

Structures of carbon catabolite protein A–(HPr-Ser46-P) bound to diverse catabolite response element sites reveal the basis for high-affinity binding to degenerate DNA operators

Maria A. Schumacher[1,*], Mareen Sprehe[1], Maike Bartholomae[2], Wolfgang Hillen[2,†] and Richard G. Brennan[1,*]

[1]Department of Biochemistry and Molecular Biology, University of Texas MD. Anderson Cancer Center, Houston, TX 77030, USA and [2]Lehrstuhl für Mikrobiologie, Institut für Biologie der Friedrich-Alexander-Universität Erlangen-Nürnberg, Staudtstr. 5, 91058, Erlangen, Germany

Received October 5, 2010; Revised November 1, 2010; Accepted November 2, 2010

ABSTRACT

In Gram-positive bacteria, carbon catabolite protein A (CcpA) is the master regulator of carbon catabolite control, which ensures optimal energy usage under diverse conditions. Unlike other LacI-GalR proteins, CcpA is activated for DNA binding by first forming a complex with the phosphoprotein HPr-Ser46-P. *Bacillus subtilis* CcpA functions as both a transcription repressor and activator and binds to more than 50 operators called catabolite response elements (*cre*s). These sites are highly degenerate with the consensus, WTGNNARCGNWW WCAW. How CcpA–(HPr-Ser46-P) binds such diverse sequences is unclear. To gain insight into this question, we solved the structures of the CcpA–(HPr-Ser46-P) complex bound to three different operators, the synthetic (syn) *cre*, *ackA2 cre* and *gntR-down cre*. Strikingly, the structures show that the CcpA-bound operators display different bend angles, ranging from 31° to 56°. These differences are accommodated by a flexible linkage between the CcpA helix-turn-helix-loop-helix motif and hinge helices, which allows independent docking of these DNA-binding modules. This flexibility coupled with an abundance of non-polar residues capable of non-specific nucleobase interactions permits CcpA–(HPr-Ser46-P) to bind diverse operators. Indeed, biochemical data show that CcpA–(HPr-Ser46-P) binds the three *cre* sites with similar affinities. Thus, the data reveal properties that license this protein to function as a global transcription regulator.

INTRODUCTION

Bacteria use carbon sources in a hierarchical manner, which ensures that the energy source most beneficial for survival is utilized preferentially. This mechanism, called carbon catabolite control, is primarily carried out at the level of transcription (1–6). In Gram-positive bacteria, carbon catabolite control is mediated in large part by the carbon catabolite protein A (CcpA), a global transcriptional regulator (7). CcpA is a member of the LacI-GalR family of transcription regulators, which are characterized by the presence of an N-terminal, approximately 60 residue DNA-binding domain and a larger effector binding, oligomerization C-terminal domain (C-domain) (8–14). Small molecules, either inducers or corepressors, bind in a cavity between two sub-domains that comprise the C-domain to regulate DNA binding (9–10,12–14). These small molecules lock the C-domain into either a closed or open conformational state. In the closed state, interactions between the DNA-binding hinge regions are stabilized allowing them to fold in the presence of cognate DNA to form the DNA binding 'hinge helices' (9–10). The finding that mutants unable to produce fructose-1,6-bisphosphate do not exhibit carbon catabolite control, led to the discovery that instead of a small

*To whom correspondence should be addressed. Tel: 713 834 6392; Fax: 713 834 6397; Email: maschuma@mdanderson.org
Correspondence may also be addressed to Richard G. Brennan. Tel: 713 834 6390; Fax: 713 834 6397; Email: rgbrenna@mdanderson.org
†M.A.S., M.S., M.B. and R.G.B. wish to dedicate this work to the memory of their dear friend and colleague, Prof. Wolfgang Hillen, who died unexpectedly and far too soon on 17 October 2010.

molecule, CcpA binds a protein as its effector. Specifically, CcpA binds the Ser46 phosphorylated form of histidine-containing phosphocarrier protein (HPr) (15). HPr is the energy coupling protein of the phosphoenolpyruvate-dependent carbohydrate:phosphotransferase system (PTS), which transports selected carbohydrates into the cell. But in the presence of high concentrations of glucose, HPr is phosphorylated on Ser46, allowing the phosphoprotein to bind CcpA and exert carbon catabolite control (15–20). The structure of a *B. megaterium* CcpA–(HPr-Ser46-P)-catabolite response element (*cre*) complex revealed that although HPr-Ser46-P binds to a region of CcpA > 30 Å from the DNA, this phosphoprotein stabilizes the closed state of the CcpA C-domains and induces relocation of key residues located at the interface of the DNA-binding and C-domains. The ultimate outcome is a juxtaposition of the CcpA DNA-binding domains that allows the 2-fold-related hinge helices to fold in the presence of cognate DNA and make key minor groove interactions at a conserved CpG step as well as positioning the helix-turn-helix (HTH) motif for major groove binding (11).

In *Bacillus subtilis*, carbon catabolite control by CcpA has been studied extensively and the data indicate that ~10% of the genome responds directly or indirectly to CcpA, underscoring its vital metabolic role (21). The multiple genes regulated by CcpA encode proteins involved in carbon metabolism and utilization, including enzymes, transporters and transcription factors (21). To carry out this regulation, CcpA acts as both a repressor and an activator. The genes activated by CcpA include *ackA* and *pta*, which are involved in the formation of acetate. CcpA–(HPr-Ser46-P) also triggers expression of the *ilv-leu* operon, which is involved in the biosynthesis of branched chain amino acids. Genes that are directly repressed by CcpA include those involved in carbon, nitrogen and phosphate metabolism (4–6). Thus, CcpA plays a central role in the coordinated regulation of catabolism and anabolism to ensure optimal cell growth under varying environmental conditions. To carry out its global role as a transcription regulator, CcpA–(HPr-Ser46-P) binds to a number of diverse *cre* sites in target promoters and genes. Interestingly, the location of *cre* site(s) within each promoter varies and correlates with whether CcpA functions as a repressor or an activator (4). For example, promoters with upstream *cre* sites such as *ackA* and *pta* appear to be primarily activated by CcpA (22–25). In contrast, promoters with overlapping *cre* sites such as *amyE*, *bglP*, *ccA*, *cdtP*, *glpF*, *phoP* and *acuA* are repressed (26–32). When bound at these locations, CcpA–(HPr-Ser46-P) apparently interferes with binding of the transcription machinery. By binding to *cre* sites located far downstream of the transcription initiation site, such as in the case of the *gnt* operon, CcpA–(HPr-Ser46-P) functions as a roadblock, again leading to transcription repression (4, 33). However, there may be exceptions in these location specific effects. For instance, CcpA–(HPr-Ser46-P) binding upstream of the promoter in the levanase operon appears to prevent transcription (34).

cre sites are highly degenerate pseudo-palindromes with the consensus sequence, $W_1T_2G_3N_4N_5A_6R_7C_8G_9N_{10}W_{11}W_{12}W_{13}C_{14}A_{15}W_{16}$ (where W stands for A or T, R for A or G and N for any base) (4,35,36). The lack of stringent sequence conservation in the *in vivo cre* sites suggests that CcpA–(HPr-Ser46-P) can bind sites with a high degree of plasticity. Consistent with this, examination of the experimentally verified *cre* sites reveals that the central CpG step and the G-C base pair at position 3 are the only completely conserved nucleotides. How CcpA binds such a diverse set of operator sites and the affinity with which CcpA binds these sites is unknown. To gain insight into these questions we carried out binding studies on *B. subtilis* CcpA–(HPr-Ser46-P) and three distinct *cre* sites; the synthetic (syn) *cre*, *ackA2 cre* and *gntR-down cre* and determined the structures of these complexes by X-ray crystallography.

MATERIALS AND METHODS

Purification of *B. subtilis* CcpA and HPr-Ser46-P

The *B. subtilis ccpA* gene, fused to a C-terminal hexahistidine (His_6)-tag encoding sequence, was subcloned via XbaI/BamHI into pET3c (Novagen) producing pWH653 (Table 1) (37). BL21(DE3) cells were transformed with the pWH653 expression vector and protein expression was induced by the addition of IPTG to a final concentration of 1 mM. The resulting cells were suspended in buffer A (20 mM Tris–HCl, pH 7.5, 300 mM NaCl, 10 mM imidazole, pH 8.0) and incubated with 5 μg/ml protease inhibitor cocktail tablets (Roche) for 20 min. After cell disruption via microfluidizer the supernatant was loaded onto a Ni^{2+}-NTA column and the protein purified using a step gradient between buffer A and buffer B (20 mM Tris–HCl, pH 7.5, 300 mM NaCl, 500 mM imidazole, pH 8.0). CcpA-containing fractions were pooled and concentrated in the presence of 5% glycerol. The protein was purified further using size exclusion chromatography (S200 column) in buffer C (20 mM Hepes, pH 7.5, 150 mM NaCl, 3 mM EDTA, 5% glycerol).

Bacillus subtilis HPr was expressed in *Escherichia coli* FT1/pLysS/pWH466 as previously described (37). Cells containing the expressed protein were suspended in buffer D (10 mM Tris–HCl, pH 7.5) and incubated with 5 μg/ml RNase, 10 μg/ml DNase and protease inhibitor cocktail tablets (Roche) for 20 min. After cell disruption the lysate was heated to 70°C and centrifuged at 20 000 rpm for 60 min. The partially purified HPr from the supernatant was phosphorylated using HPr kinase as

Table 1. Strains and plasmids

Strains/plasmid	Characteristics	Reference
Escherichia coli FT1/pLysS	BL21(DE3) Δ (*ptsHIcrr*)/pLys, Km^R, Cm^R	56
Plasmids		
p4813	Amp^R, *ptsK*	57
pWH466	pET3c, *ptsH* (*B. subtilis*)	37
pWH653	pET3c, *ccpA(his)$_6$* (*B. subtilis*)	39

described previously (19). The resulting phosphorylated protein, HPr-Ser46-P, was subjected to anion exchange chromatography on a Sepharose QFF column using a linear gradient between buffer D and buffer E (10 mM Tris–HCl, pH 7.5, 1 M NaCl). HPr-Ser46-P containing fractions were pooled and concentrated using an Amicon Ultra 3 kDa filter. A final purification step was performed using an S75 column (GE Healthcare). For the surface plasmon resonance (SPR) measurements glycerol free HBSE buffer (150 mM NaCl, 3 mM EDTA, 10 mM Hepes, pH 7.4) was used as storage buffer for both proteins since glycerol can affect the measurements.

Determination of DNA-binding affinities via fluorescence polarization

The binding affinities of CcpA for the syn *cre* (5′-CTGTT AGCGCTTTCAG-3′), *ackA*2 *cre* (5′-TTGTAAGCGTTA TCAA-3′) and *gntR-down cre* (5′-TTGAAAGCGGTACC AT-3′) were determined by fluorescence polarization (FP) at 25°C using a Beacon 2000 fluorescence polarization instrument (38). 5′-Fluorescein labelled hairpin *cre* elements, where the complementary 16 bp of the syn *cre*, *ackA2 cre* and *gntR-down cre*, were separated by a loop consisting of five cytosines, were used. For each measurement CcpA was titrated into a 1-ml reaction cell containing a buffer consisting of 150 mM NaCl, 20 mM Hepes, pH 7.4, 3 mM EDTA, 10 μg/ml poly(dIdC) and 1 nM 5′-fluorescein-labelled oligonucleotide in the presence and absence of 50 μM HPr-Ser46-P. All measurements were performed in triplicate.

Determination of DNA-binding affinities via SPR

SPR measurements were performed on a Biacore X instrument operated at 25°C (Biacore, Uppsala, Sweden). The coupling of the DNA and the measurement was carried out as described previously (39). The DNA sites used are shown in Table 2. HBS–EP buffer purchased from Biacore was used at a flow rate of 40 μl/min for all measurements since mass transport was minimal. The running buffer and each sample were supplemented with 50 μM HPr-Ser46-P during the kinetic experiments to minimize bulk effects. To ensure full saturation of the *gntR-down cre* with the protein complex, 75 μM HPr-Ser46-P was used. Titrations were carried out with 5 or 20 to 100 nM CcpA$(His)_6$. To regenerate the chip and to stop the dissociation of the CcpA–(HPr-Ser46-P)-complex from the chip, 80 μl pure HBS-EP were injected at 40 μl/min after each sample.

Crystallization of CcpA–(HP-Ser46-P) bound to the syn, *ackA2* and *gntR-down cre* sites

The *B. subtilis* CcpA–(HPr-Ser46-P) complex was crystallized in the presence of *cre* elements used in the binding studies: the syn *cre* (5′-CTGTTAGCGCTTTCA G-3′), *ackA*2 *cre* (5′-TTGTAAGCGTTATCAA-3′) or *gntR-down cre* (5′-TTGAAAGCGGTACCAT-3′). Each CcpA–(HPr-Ser46-P)–DNA complex (using a 1:2:1 ratio of CcpA dimer: HPr-Ser46-P monomer: DNA duplex) was mixed with various reservoir solutions and crystallized using the hanging drop vapor diffusion method. Notably, different conditions were required to obtain each of the crystals. Crystals of the CcpA–(HPr-Ser46-P)–syn *cre* were obtained by mixing the complex 1:1 (v:v) with a reservoir of 20% PEG 3350 and 0.2 M ammonium formate. Crystals of the CcpA–(HPr-Ser46-P)–*ackA*2 complex were grown by mixing the complex 1:1 with a reservoir of 17.5% PEG 8000, 0.2 M ammonium sulphate, 0.01 M magnesium chloride, 0.05 M MES pH 5.6. Crystals of the CcpA–(HPr-Ser46-P)–*gntR-down cre* complex were produced by mixing the complex 1:1 with a reservoir of 20% PEG 6000, 0.1 M citric acid, pH 5.0. Despite the different requirements for obtaining the crystals, all three took the space group $P2_12_12_1$. The crystals were cryoprotected for data collection by supplementing the reservoirs with 25%, 25% and 20% glycerol, respectively, and dipping each crystal for several seconds in the cryoprotectant before looping and placing in the cryostream. X-ray intensity data were collected at the Advanced Light Sources (ALS, Berkeley, CA, USA) beamline 8.2.1 (Table 3).

Structure determination and refinement

All three structures were solved by molecular replacement with MolRep using the same starting model, 2FEP [the *B. subtilis* CcpA (residues 60–334)–(HPr-Ser46-P) structure] (11,40). After rigid-body refinement in CNS, clear electron density for the DNA-binding region, residues 1–59, and the DNA was revealed. The *cre* sites and DNA-binding residues 2–59 were then built into their respective densities and positional (*xyz*) refinement was carried out. The 5′–3′ directions of the DNA sites were ascertained by examination of the electron density and R_{free}. After several rounds of refinement and extensive rebuilding, *xyz* and thermal parameter (B factor) refinement was utilized for the CcpA–(HPr-Ser46-P)–*ackA2* and CcpA–(HPr-Ser46-P)–syn structures (41,42). The final

Table 2. Oligonucleotides

Oligonucleotide	Sequence (5′→3′)	Modification	Reference
ackA_cre2_fw	TTCTTATTGTAAGCGTTATCAATACG	5′ biotinylated	This work
ackA_cre2_rev	CGTATTGATAACGCTTACAATAAGAA		This work
gntR_cre_fw	GTCTGATTGAAAGCGGTACCATTTTA	5′ biotinylated	This work
gntR_cre_rev	TAAAATGGTACCGCTTTCAATCAGAC		This work
syn_cre_fw	TTCTTACTGTTAGCGCTTTCAGTACG	5′ biotinylated	This work
syn_cre_rev	CGTACTGAAAGCGCTAACAGTAAGAA		This work
Non-specific DNAfw	AATCATTTATGGCATAGGCAACAAGT	5′ biotinylated	37
Non-specific DNArev	ACTTGTTGCCTATGCCATAAATGATT		37

Table 3. Selected crystallographic data for CcpA-(HPr-Ser46-P)-DNA structures

DNA site used in complex	syn *cre*	*ackA2 cre*	*gntR-down cre*
DNA site	CTGTTAG**CG**CTTTCAG[a]	TTGTAAG**CG**TTATCAA	TTGAAAG**CG**GTACCAT
DNA bend angle (°)	31.0	56.0	41.0
Space group	$P2_12_12_1$	$P2_12_12_1$	$P2_12_12_1$
Cell dimensions (Å)	$a = 74.1$; $b = 105.2$; $c = 173.3$	$a = 74.2$; $b = 103.5$; c = 176.7	$a = 73.9$; $b = 103.5$; $c = 175.3$
Resolution (Å)	105.41–2.97	103.70–2.95	87.71–3.30
Overall R_{sym}(%)[b]	6.5 (46.3)[c]	8.8 (43.6)	12.5 (49.1)
Overall $I/\sigma(I)$	16.5 (1.6)	13.8 (2.2)	8.1 (2.1)
No. of total reflections	93 430	99 250	89 855
No. of unique reflections	28 545	29 339	19 982
Refinement statistics			
Resolution (Å)	105.4.0–2.97	103.70–2.95	87.71–3.30
R_{work}/R_{free}(%)[d]	21.2/26.9	21.7/27.2	22.1/27.6
RMSD			
Bond angles (°)	1.20	1.20	1.26
Bond lengths (Å)	0.007	0.007	0.008
Ramachandran analysis			
Most favoured (%/#)	80.5/599	83.1/618	81.8/609
Add. allowed %/#)	17.6/131	15.6/116	17.0/120
Gen. Allowed (%/#)	1.3/10	0.9/7	1.9/14
Disallowed (%/#)	0.5/4	0.4/3	0.3/2

[a]The underlined G, C and bold CG are the only sequences completely conserved amongst characterized *cre* sites in *Bacillus subtilis*.
[b]$R_{sym} = \Sigma\Sigma|Ihkl - Ihkl(j)|/\Sigma Ihkl$, where $Ihkl(j)$ is observed intensity and $Ihkl$ is the final average value of intensity.
[c]Values in parentheses are for the highest resolution shell.
[d]$R_{work} = \Sigma||F_{obs}|-|F_{calc}||/\Sigma|F_{obs}|$ and $R_{free} = \Sigma||F_{obs}|-|F_{calc}||/\Sigma|F_{obs}|$; where all reflections belong to a test set of 5% randomly selected data.

CcpA–(HPr-Ser46-P)–*ackA2* structure includes all 32 nt of the DNA duplex, residues 2–333 of each CcpA subunit, residues 2–88 of each HPr-Ser46-P molecule, four sulphate molecules and 46 solvent molecules. The final CcpA–(HPr-Ser46-P)–syn structure includes all nucleotides of the DNA duplex, residues 2–333 of each CcpA subunit, residues 2–88 of each HPr-Ser46-P molecule and 49 solvent molecules. The final CcpA–(HPr-Ser46-P)–*gntR-down* structure includes all nucleotides of the DNA duplex, residues 2–333 of each CcpA subunit and residues 2–88 of each HPr-Ser46-P molecule. Selected data collection and refinement statistics are given in Table 3.

RESULTS AND DISCUSSION

CcpA–(HPr-Ser46-P) binding to the syn, *ackA2* and *gntR-down cre* sites

Bacillus subtilis CcpA–(HPr-Ser46-P) has been shown to bind to a number of diverse *cre* operators, however, there is no information regarding its relative binding affinities for these sites. Hence, we began our study by determining the equilibrium binding constants (K_d's) of CcpA–(HPr-Ser46-P) for three well-studied *cre* sites, the synthetic (syn) *cre*, *ackA2 cre* and the *gntR-down cre* (Figure 1A). The syn *cre* is an artificial operator that binds the *B. megaterium* CcpA–(HPr-Ser46-P) complex with high affinity and was used in structure determination of the *B. megaterium* CcpA–(HPr-Ser46-P)–DNA complex (11). Given that *B. megaterium* and *B. subtilis* CcpA proteins share 76% sequence identity, we hypothesized that the *B. subtilis* CcpA–(HPr-Ser46-P) complex would also bind the syn *cre* with high affinity. Indeed, using a fluorescence polarization (FP)-based DNA-binding assay, we determined that *B. subtilis* CcpA–(HPr-Ser46-P) bound the 16-bp syn *cre* (5′-CTG TTAGCGCTTTCAG-3′) with a K_d of 10 ± 1 nM (Figure 1B). As has been shown previously, high-affinity binding to *cre* DNA requires HPr-Ser46-P. In accord, in the absence of HPr-Ser46-P, CcpA bound the syn *cre* with 100-fold reduced affinity ($K_d = 1020 \pm 110$ nM) (Supplementary Figure S1A).

The *ackA2 cre* is one of two *cre* sites in the promoter of the gene encoding acetate kinase (31). *ackA2* and the second *cre* site, called *ackA1*, are centered at 22 and 82 bp, respectively, upstream of the −35 box and differ from each other in four positions in the right-half site of the operator (*ackA1*: 5′-TTGTAAGCGTTCATCA-3′, *ackA2*; 5′-TTGTAAGCGTTATCAA-3′). However, only the *ackA2 cre* plays a role for CcpA-dependent carbon catabolite activation of *ackA*, while the *ackA1 cre* is not required (31). The *ackA2 cre* differs from the syn *cre* in 5 nt positions (Figure 1A), yet CcpA–(HPr-Ser46-P) bound the *ackA2 cre* with essentially the same affinity (K_d, 6.4 ± 1 nM, Figure 1B). Again, the absence of HPr-Ser46-P resulted in a significant, >100-fold reduction in binding with a $K_d = 950 \pm 90$ nM (Supplementary Figure S1B).

Similar to *ackA*, the *gntR* operon is regulated by two putative *cre* sites. However, in this case one site, *gntR-down* is located within a gene, specifically, the first gene of the *gnt* operon. The second putative *cre*, *gntR-up* is located in the promoter region. While *gntR-down* was shown to be bound by CcpA–(HPr-Ser46-P), *gntR-up* showed no interaction with the complex, as ascertained by DNase I protection studies (43). The *gntR-down cre* diverges from the syn *cre* in seven of 16 positions and four of 16 positions when compared to the *ackA2 cre*

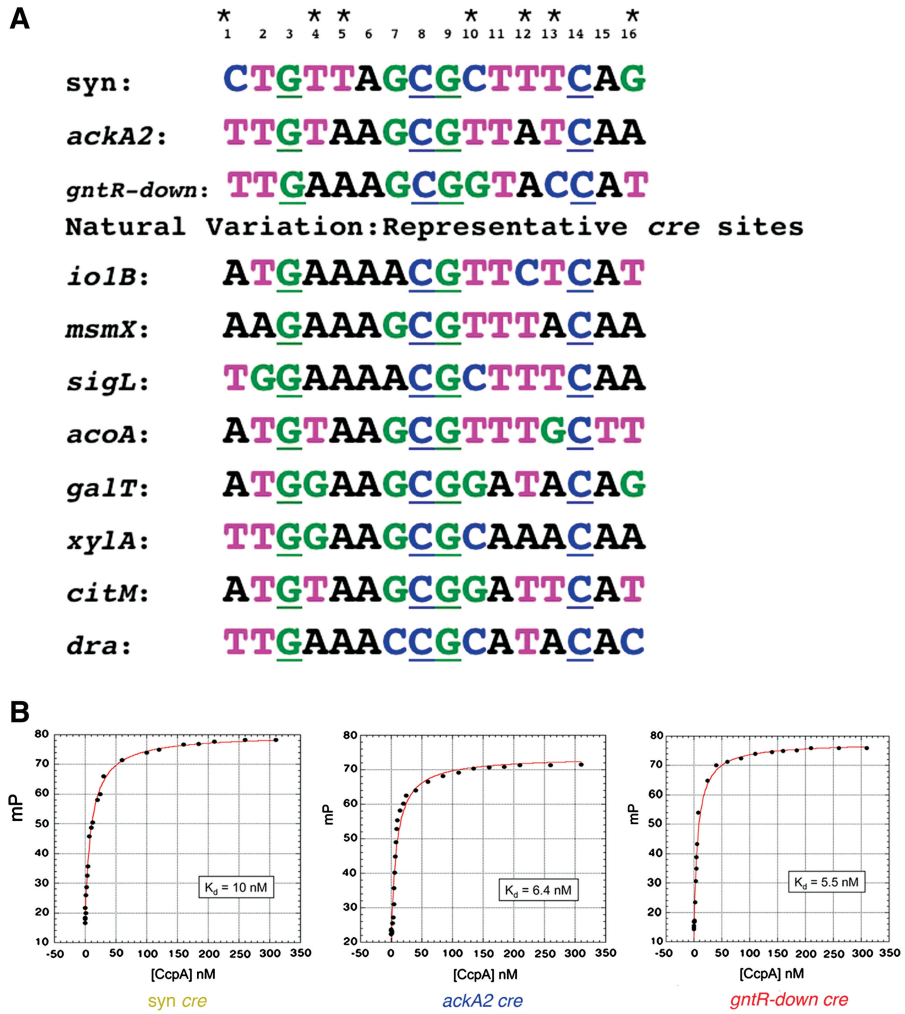

Figure 1. CcpA–(HPr-Ser46-P)–*cre* site promiscuity. (**A**) Sequences of the three *cre* sites, syn, *ackA2* and *gntR-down*, used in the study. Asterisks over the sequences show the locations where the sites differ. Below the three sites used in the study are eight additional *cre* sites. These sequences are shown to illustrate the natural variation of *in vivo cre* sites (36,50–54). (**B**) Fluorescence polarization-based binding isotherms of CcpA–(HPr-Ser46-P) syn *cre*, *ackA2 cre* and *gntR-down cre* (from left to right). The K_d calculated for each experiment is indicated in each isotherm.

(Figure 1A). But again, binding studies demonstrated that CcpA–(HPr-Ser46-P) bound this site with essentially the same K_d, 5.2 ± 0.2 nM, as the syn and *ackA2 cre* sites (Figure 1B). Moreover, this binding was dependent on HPr-Ser46-P as the K_d of CcpA alone for this site was 900 ± 60 nM (Supplementary Figure S1C).

Given the significant differences in the sequences of the syn, *ackA2* and *gntR-down* sites, the finding that CcpA–(HPr-Ser46-P) bound these sites with the same K_d was surprising. Thus, we determined K_d's from the rate constants of CcpA–(HPr-Ser46-P) binding to the *ackA2 cre*, *syn cre* and *gntR-down cre* using SPR. For these studies, 4000 RU (Response Units) of Neutravidin, a streptavidin analogue, were coupled to a CM5-chip. Subsequently, 5′ biotinylated *cre*-DNA was coupled in flowcell 2 and 5′ biotinylated reference DNA was in flowcell 1. As reported previously, 50 μM HPr-Ser46-P was contained in the running buffer to observe only the dissociation of the CcpA–(HPr-Ser46-P) complex from the DNA (39). The kinetics were analysed via titration of 5 or 20 to 100 nM CcpA and 50 μM HPr-Ser46-P (Supplementary Data). All data were fitted with the BIAEVALUATION software 3.1 to calculate the association and dissociation rate constants from the sensorgrams. Representative sensorgrams with the calculated best fits are shown in Figure 2 and the resulting rate constants are given in Table 4. The binding constants were highly congruent with those obtained by FP studies. Specifically, the K_d's for CcpA–(HPr-Ser46-P) binding to the syn, *ackA2* and *gntR-down cre* sites were 3.8 ± 0.1, 1.6 ± 0.4, 3.0 ± 0.4 nM, respectively (Figure 2). Thus, only small differences in the K_d's were observed between the two studies, likely due to different buffer conditions and oligodeoxynucleotide lengths. However, the critical finding is that both studies demonstrate that CcpA–(HPr-Ser46-P) complex binds the three diverse *cre* sites with essentially the same affinity. To understand the molecular mechanisms by which CcpA–(HPr-Ser46-P) can interact with high affinity to such divergent *cre* sequences we determined crystal structures of the three complexes.

Structure determination of *B. subtilis* CcpA–(HPr-Ser46-P)–*cre* complexes

For structural studies, we crystallized CcpA–(HPr-Ser46-P) with 16-bp oligodeoxynucleotides containing the three different *cre* sites used in the FP-binding studies; the syn *cre* (5′-CTGTTAGCGCTTTCAG-3′), the *ackA2 cre* (5′-TTGTAAGCGTTATCAA-3′) and the *gntR-down cre* (5′-TTGAAAGCGGTACCAT-3′). The DNA sites were designed to be the same length in hopes that the crystals would adopt similar packing environments, thus permitting a direct comparison of the structures. Interestingly, different conditions were required to produce each crystal. However, the crystals all took the orthorhombic space group, $P2_12_12_1$, and had very similar cell edges and crystal packing. The CcpA–(HPr-Ser46-P)–syn, CcpA–(HPr-Ser46-P)–*ackA2* and CcpA–(HPr-Ser46-P)–*gntR-down* structures were solved and refined to R_{work}/R_{free} values of 21.2%/26.9%, 21.7%/27.2% and 22.1%/27.6% to 2.97 Å, 2.95 Å and 3.30 Å, respectively (Table 3; 'Materials and Methods' section). Each structure contains a CcpA dimer, two HPr-Ser46-P molecules and an entire DNA duplex in the crystallographic asymmetric unit (ASU). The presence of an entire dimer bound to a DNA duplex in the ASU allowed an unfettered comparison of the structures, as there is no 2-fold disorder in the DNA or protein to complicate our structure analyses.

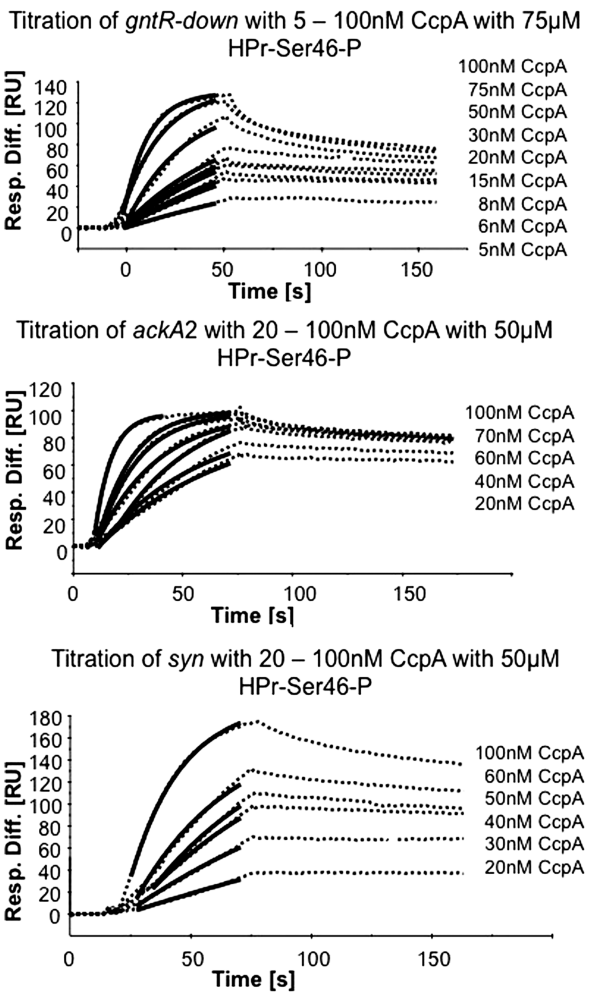

Figure 2. SPR analysis of CcpA–(HPr-Ser46-P) binding to *cre* elements reveals similar association and dissociation rates. The titrations were carried out with 5 or 20 to 100 nM CcpA. To reduce bulk effects, the running buffer was supplemented with 75 µM HPr-Ser46-P in the *gntR-down cre* experiment (**A**) and with 50 µM HPr-Ser46-P in the *ackA2* and *syn cre* experiments (**B** and **C**). Under these conditions, CcpA is completely bound by HPr-Ser46-P (39). Dashed lines represent the measured data and bold lines are the best calculated fits for the association reactions.

Overall structures of CcpA–(HPr-Ser46-P)–*cre* complexes

The overall structures of the CcpA–(HPr-Ser46-P)–*cre* complexes show that HPr-Ser46-P binds the surface of CcpA with a stoichiometry of one HPr-Ser46-P molecule per CcpA subunit, as previously observed in the *B. megaterium* CcpA–(HPr-Ser46-P)–*cre* structure (Figure 3) (11). The three *B. subtilis* CcpA–(HPr-Ser46-P) complexes can be superimposed onto the *B. megaterium* CcpA–(HPr-Ser46-P) complex with root mean square deviations (RMSDs) ranging from 2.4 Å to 2.6 Å for all Cα atoms, including both CcpA subunits and both HPr-Ser46-P molecules (Supplementary Figure S2). Like *B. megaterium* CcpA and other LacI-GalR family members, *B. subtilis* CcpA is composed of an N-terminal DNA-binding domain (residues 1–59) and a C-terminal dimerization/HPr-Ser46-P-binding domain (residues 60–334) (7–12). The DNA-binding domain has two distinct DNA-binding elements or modules; a three-helix bundle, herein referred to as the helix-turn-helix-loop-helix (HTHLH), where helices 1 and 2 form the major groove binding helix-turn-helix motif (HTH) (helix 1: residues 5–12, helix 2: residues 16–24, helix 3: residues 31–44) and the hinge helix, helix 4 (residues 50–58), which inserts into the minor groove of the central CpG step, thereby kinking the DNA (Figure 3). The CcpA C-domain can be divided into two structurally

Table 4. Association and dissociation rate constants and equilibrium binding constants of the CcpA–(HPr-Ser46-P) complex for *cre* sites

	K_a (M^{-1} s^{-1})	K_d (s^{-1})	K_D (M)	χ^{2a}
ackA2	$6.0 \pm 1.9 \times 10^5$	$9.5 \pm 1.0 \times 10^{-4}$	$1.6 \pm 0.4 \times 10^{-9}$	3.5–4.4
gntR-down	$6.0 \pm 1.7 \times 10^5$	$1.8 \pm 0.3 \times 10^{-3}$	$3.0 \pm 0.4 \times 10^{-9}$	3.4–5.2
syn	$3.2 \pm 0.6 \times 10^5$	$1.2 \pm 0.2 \times 10^{-3}$	$3.8 \pm 0.1 \times 10^{-9}$	5.8

[a]χ^2 is the average deviation.

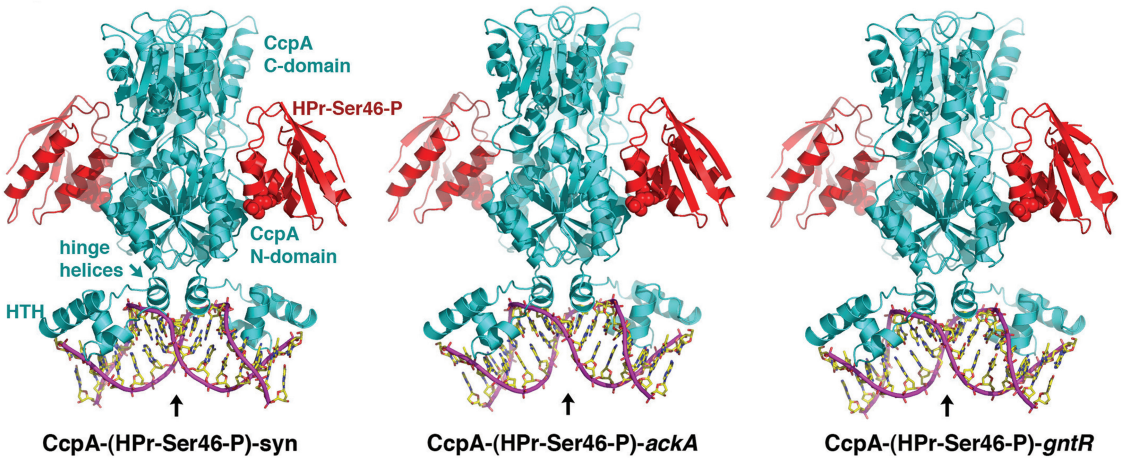

Figure 3. Structures of CcpA–(HPr-Ser46-P) bound to three *cre* sites. Shown from left to right are the ribbon diagrams of the CcpA–(HPr-Ser46-P)–syn, CcpA–(HPr-Ser46-P)–*ackA2* and CcpA–(HPr-Ser46-P)–*gntR-down* structures. The CcpA subunits in the dimer are coloured cyan, the HPr-Ser46-P molecules are coloured red. The α-helices are shown as coils and β-strands as arrows. The DNA is shown as sticks with phosphorus, nitrogen, oxygen and carbon atoms coloured magenta, blue, red and yellow, respectively. Each DNA phosphate backbone is depicted as a magenta tube. The Ser46-P residues are shown as solid surface representations. This figure, Figures 4A–C, 5A and B and 6 were made with PyMOL (55).

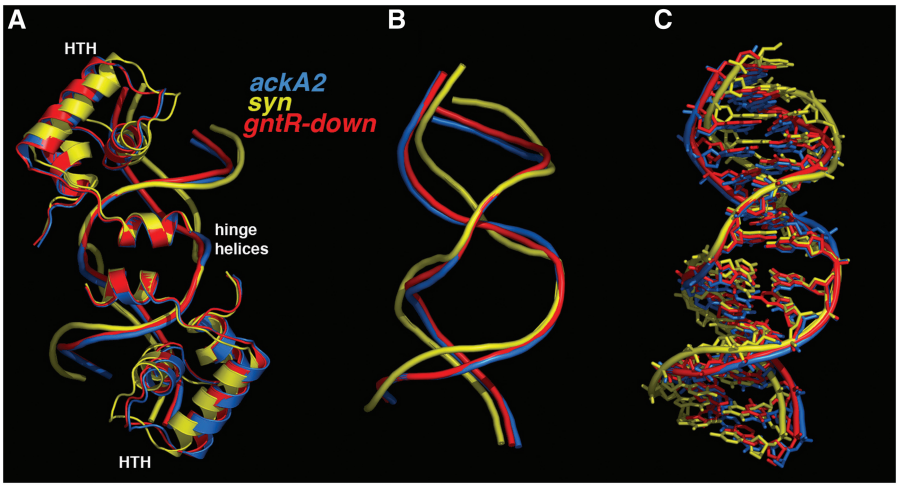

Figure 4. CcpA–(HPr-Ser46-P)–*cre* binding requires protein and DNA flexibility. Different orientations of the HTHLH modules and the DNA conformations of CcpA–(HPr-Ser46-P) bound *cre* sites. (**A**) View of the DNA-binding HTHLH modules and cognate DNA sites after superimposition of the hinge helix and C-domain of CcpA of each structure. Note that the positions of the HTH motifs are significantly different with the greatest change seen for the HTH motif of the CcpA bound to the syn *cre* (yellow). The structures of the HTHLH, hinge helices and DNA backbones of the CcpA–(HPr-Ser46-P)–*ackA2* and CcpA–(HPr-Ser46-P)–*gntR-down* complexes are coloured blue and red, respectively. (**B**) View of the superimposed DNA phosphate backbones of the *cre* sites, coloured as in Figure 4A and rotated ~45° to allow a view into the enlarged DNA minor grooves. (**C**) View of the overlaid *cre* DNAs with all atoms included. Coloured as in Figure 4A.

similar subdomains, the N-subdomain and the C-subdomain. The N-subdomain consists of a six-stranded parallel β-sheet, surrounded by four α-helices. The C-sub-domain contains a five β-stranded parallel sheet and five surrounding α-helices. The subdomains are connected by three crossovers that can act as a joint to permit rotation of the two subdomains. The CcpA dimerization interface is extensive and buries 3900 Å^2 surface area from solvent.

CcpA–(HPr-Ser46-P)–*cre* structures: plasticity in DNA binding

The three CcpA–(HPr-Ser46-P)–*cre* complexes are similar in overall structure and arrangement, however, there are some notable differences (Figures 3 and 4A). In particular, an analysis of the DNA structure using Curves+ (44) reveals that whilst the syn *cre* site is bent by 31° when bound by CcpA–(HPr-Ser46-P), the *ackA2* and *gntR-down cre* sites are bent by 56° and 41°, respectively (Figure 4B and C). In addition, the syn *cre* DNA minor groove has a greater width, 13.1 Å, than either of those of the *ackA2* and *gntR-down cre*s, which have minor groove widths of 12.3 Å and 12.4 Å, respectively. Consistent with the differences in DNA structural distortions, the CcpA DNA-binding domains display differences in their relative conformations. This is readily observed in superimpositions, which show that whilst the overlay of CcpA residues 50–330, which contains the hinge helices and

C-domains, results in rmsds between 0.3 Å and 0.4 Å, inclusion of residues 2–49 results in RMSDs of 0.9 Å and 1.0 Å when comparing subunits from the CcpA–(HPr-Ser46-P)–syn structure to those from the CcpA–(HPr-Ser46-P)–*ackA2* and CcpA–(HPr-Se46-P)–*gntR-down* structures, respectively. In contrast, the superimposition of residues 2–330 of the *ackA2* and *gntR-down* CcpA subunit structures results in an rmsd of only 0.45 Å, which is within the experimental error of the coordinates (~0.50 Å from the Luzzati plot analysis). These comparisons indicate that the HTHLH DNA-binding module, residues 2–49, of the syn bound structure displays an altered conformation relative to the corresponding HTHLH modules from the *ackA2* and *gntR-down* bound structures (Figure 4A). This difference involves a rigid-body movement of the HTHLH unit because superimpositions of the individual HTHLH units show that they are essentially identical in all three structures (the HTHLH motifs can be superimposed with rmsds of 0.3–0.4 Å). The HTHLH of both subunits of the syn bound structure undergo the same relative shift (Figure 4A). The flexible attachment by residues 45–50 of the HTHLH unit to the hinge helices appears important in permitting this rigid-body movement and requires the ability of residues 45–50 to take multiple conformations. Such an ability to rotate allows the HTHLH modules to adjust to different DNA conformations and hence allows optimal docking of the HTH units onto the DNA major groove (Figure 4A).

Interestingly, there are no data that would suggest why the sequences of the *ackA2* and *gntR-down cre* sites would display larger bend angles compared to the syn sequence (45). The smaller overall bend in the syn bound site appears necessary for permitting the specific interaction of the HTH motif, which is located closer to the centre of the this *cre* site. Thus, it is not clear whether the altered DNA structures are the result of bend angle predispositions or are the outcome of the insertion of the CcpA–hinge helices into the central CpG step of each sequence. Regardless of the underlying cause, our structures demonstrate that CcpA is able to adjust to significant changes in DNA conformation by the inherent flexibility exhibited by the linker between its two independent DNA-binding modules, the HTHLH and hinge helices.

Flexibility between DNA-binding modules allows optimal docking

The above analysis demonstrates that CcpA can adjust to different DNA distortions because of the modularity and flexibility of its two DNA-binding elements. But this does not explain how CcpA can interact specifically with the DNA nucleobases of such diverse DNA sequences. A detailed comparison of the contacts made by CcpA to each *cre* site shows only two conserved side chain–base interactions that appear specific. These are the major groove contacts from HTH residue Arg22 to Gua3 (two guanidinium side chain hydrogen bonds to the O6 and N7 atoms of Gua3) and hinge-helix residue Leu56 to the CpG step in the DNA-minor groove (Figure 5). These two interactions precisely anchor or dock the HTHLH and the hinge helix onto the major and minor grooves of the *cre* DNA site, respectively. While the Arg22 to guanine contact is a 'standard' type of specificity determining interaction that has been observed in multiple protein–DNA complexes, the Leu56–hinge helix interaction with the highly rolled central CpG step (roll angles range from 44° to 45°) is unusual (Figure 5A and B). The formation of this interaction is likely a multistep, complex process, as it requires the coupling of DNA distortion with hinge helix folding and leucine insertion into the minor groove. In the CcpA apo state, the hinge region exists in an unfolded state (11). Hence, to form the interaction, the hinge helices must form and the folding is likely coupled to CpG distortion. Interestingly, in all the structures, hinge helix backbone atoms make weak (non ideal geometry) but specific hydrogen bonds to the nucleobases of the central CpG step; the carbonyl oxygen of Ala53 and the amide nitrogen of Ala57, interact with the Gua N2 and Cyt O2 atoms, respectively (range of hydrogen bond distances in the three structures are; Gua(N2)-Ala53(C = O): 3.1 Å to 3.4 Å and Cyt(O2)-Ala57(NH2): 3.1 Å to 3.6 Å) (Figure 5B). These contacts would favour coupled helix folding with DNA distortion and also impart a preference for a CpG step. Finally, hinge helix folding precisely orients the 2-fold-related Leu56 residues to insert into the widened minor groove. The perfect fit of the Leu56 residues into this space provides side chain specificity (Figure 5B). Indeed, this leucine is completely conserved in all CcpA proteins and all characterized LacI-GalR proteins that utilize hinge helices to bind DNA (9,11,14).

As would be expected if they play essential roles in DNA binding, Arg22 and Leu56 are conserved in all CcpA proteins (11). Moreover, Gua3, its 2-fold-related counterpart, and the central CpG step are the only completely conserved bases amongst the more than 50 identified *B. subtilis cre* sequences. Studies have demonstrated that these two base pairs are essential for transcription regulation by CcpA (Figure 1A) (4,35). In particular, Weickert and Chambliss carried out a detailed analysis on the affect of site-directed mutagenesis of the *cre* site on catabolite repression of the *B. subtilis* amylase operon (35). Their studies underscored the significant flexibility in the operator sequence and revealed the consensus, **TG_3WA*ANC_8G_9NTNWC_{14}**A (where bolded letters represents the most critical bases and the A* indicates the transcription start site) (35). Thus, aside from the conserved guanine/cytosine base pairs at positions 3/14 and 8/9, the only other position that shows a strong preference for specific nucleotides are Thy2 and its 2-fold-related nucleotide, Ade15 (Figure 1A). Our current structures show that the methyl groups of Thy2A (and Thy15B) are contacted by the Cβ atom of residue Asn29 from each subunit. Asn29 is completely conserved amongst CcpA proteins. Interestingly, the corresponding Asn-CβThy2 contact was not observed in the *B. megaterium* CcpA–(HPr-Ser46-P)–DNA structure, suggesting that it cannot be a CcpA specificity determining contact (11). However, Thy2 in both the *B. subtilis* and *B. megaterium* CcpA–(HPr-Ser46-P)–DNA structures contain an unusual stacking interaction with the arginine (Arg22 in *B. subtilis* and Arg21 in *B. megaterium*), which

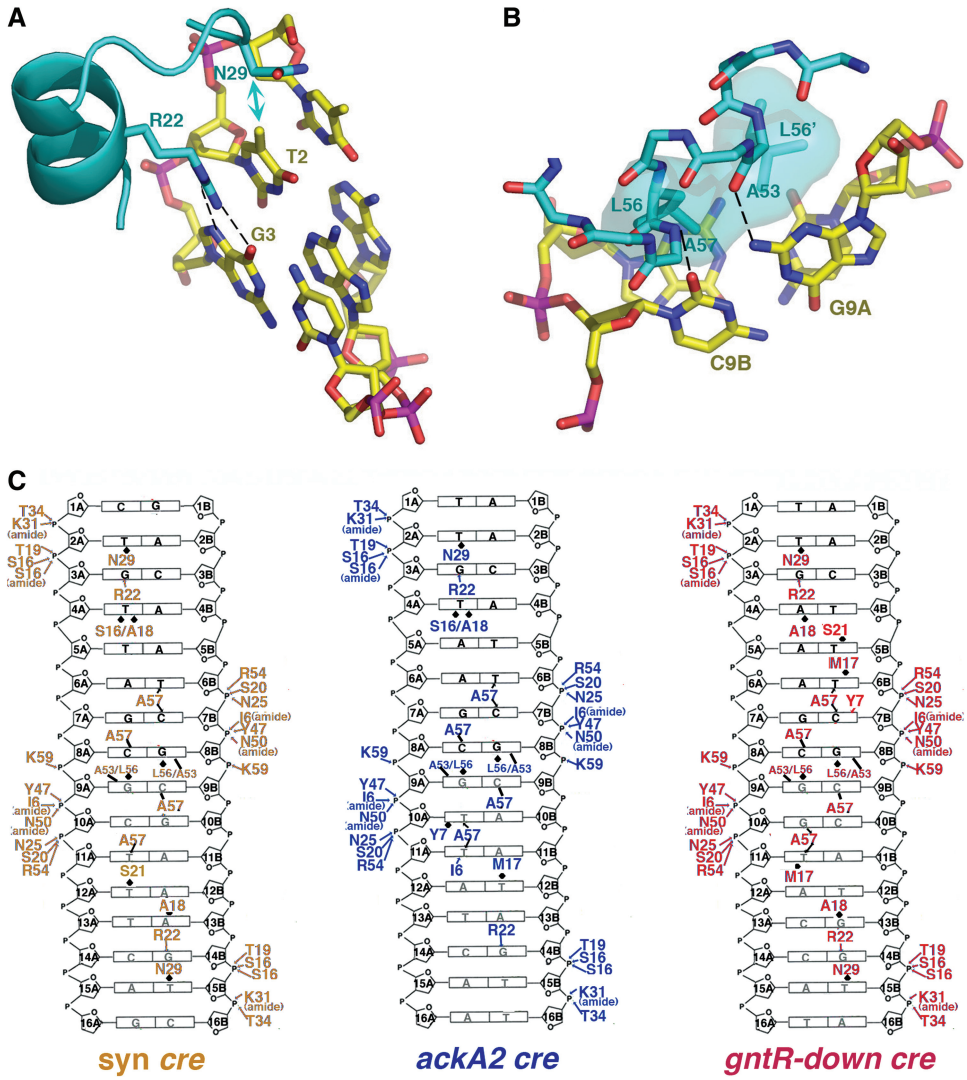

Figure 5. CcpA–*cre* interactions. (**A**) Close up view of the Arg22 interaction with Gua3 and the van der Waals contact between the side chain Cβ of Asn29 with Thy2 (indicated by double headed arrow). Also note the stacking of the Arg22 side chain with the unstacked Thy2 nucleobase. (**B**) Close up of the hinge helix interactions with the rolled CpG step (for clarity, only one of the two hinge helices is shown). Weak hydrogen bonds are observed between the carbonyl oxygen moiety of residue Ala53 to the N2 atom of Gua9 and the amide nitrogen of Ala57 and the O2 of Cyt8. The Leu56 side chains (highlighted as transparent surfaces) fit optimally into the widened minor groove. Figures 5A and B show contacts from the CcpA–(HPr-Ser46-P)–*ackA2* structure. The same interactions are observed in the CcpA–(HPr-Ser46-P)–*gntR-down* and CcpA–(HPr-Ser46-P)–syn structures. (**C**) From left to right are schematic representations of the interactions between CcpA and the syn, *ackA2* and *gntR-down* sites. The strands are labelled 1A–16A on one strand and 1B–16B on the other strand. Bases are represented as rectangles and labelled according to sequence. The ribose groups are shown as pentagons. van der Waals contacts between side chains and bases are indicated by black diamonds and hydrogen bonds, by black arrows. Hydrogen bonds to the backbone phosphate groups are shown as coloured arrows. Peptide backbone–DNA hydrogen bonds are designated further with the word 'amide' with the exception of the A53 and L56 DNA hydrogen bonds.

makes specific hydrogen bonds with the guanines at positions 3 and 14 (Figure 5A and C). This stacking/van der Waals interaction between the arginine side chain and the thymine base fits the criteria for what has been termed a 5′-pyrimidine-guanine-3′ (5′-YpG-3′) interaction (46,47). This interaction is thought to arise because of the inherent flexibility of pyridimine-guanine steps, which allows them to become unstacked more readily (48). In a 5′-YpG-3′interaction, the arginine side chain makes specific hydrogen bonds to the major groove face of the 5′-guanine nucleobase, whilst simultaneously contacting the unstacked preceding pyrimidine (48). This type of recognition mode was initially shown to be critical for the specific DNA binding of the *Saccharomyces cerevisiae* sporulation specific transcription factor, Ndt80, to the middle sporulation element (MSE) DNA site (46). A subsequent survey by the Glover lab showed that several different classes of DNA-binding motifs, from HTH to zinc fingers, utilized this mode of recognition (47). Similar to the 5′-pyrimidine of the 5′-YpG-3′ in the Ndt80-DNA structure, the Thy2 nucleobases in the *B. subtilis* CcpA–(HPr-Ser46-P)–DNA complexes all show significant displacement from optimal stacking with the following Gua3 as well as the hallmark stacking/van der Waals

contact with the side chain of Arg22 (Figure 5A). However, the Arg22-Thy2 stacking may not be as optimal (~4.1 Å) as other 5′-YpG-3′ contacts, perhaps explaining why nucleotides 2 and 13 are not completely conserved in *cre* sites. In fact, analysis of the sequences of a number of *cre* sites shows that a thymine or pyrimidine is not strictly conserved at this location and in fact, in several cases is even a purine (Figure 1A). Regardless, the Arg22-(5′-YpG-3′) interaction combined with the Asn29 Cβ contact to Thy2 likely explains why a thymine is strongly preferred at *cre* position 2 (Figure 1B).

Aside from the complete conservation of guanine–cytosine base pairs 2/14 and 8/9 and the preference for a thymine/adenine at position 2/13, the other positions of the 16-bp *cre* are not conserved in *cre* sites and have been shown not to be important for CcpA-mediated transcription regulation (Figure 1A) (4,35). The structures show that these nucleotides are not recognized specifically by any CcpA residue, providing an explanation for this finding. In fact, the contacts that CcpA makes to these nucleotides are confined to van der Waals interactions, which lack strict chemical and geometrical restraints. In mediating its DNA contacts, CcpA utilizes non-polar side chains or the aliphatic portions of polar residues (Figure 5C). The residues used in these varied contacts are Ile6, Ser16, Met17, Ala18, Ala57 and the aliphatic portions of Tyr7 and Asn29. It is also of interest to note that while CcpA makes several water-mediated DNA phosphate backbone contacts there do not appear to be any solvent bridged protein–nucleobase interactions to any of the *cre* site bases. Perhaps the van der Waals contacts act to replace these commonly found interactions.

The large number of van der Waals contacts observed in the CcpA–*cre* complexes underscores the abundance of non-polar residues in the CcpA DNA-binding domain, particularly in its recognition helix (helix 2). It also suggests one reason why most *cre* sites are relatively rich in AT base pairs as non-polar side chains can partake in favourable interactions with the major groove-protruding methyl groups of thymines. Regardless, the non-polar side chains found in the CcpA DNA-binding domains have the capability of contacting any of the four nucleobases. Comparison of the three structures shows that the number of overall side chain–base contacts are very similar; the CcpA–(HPr-Ser46-P)–syn, CcpA–(HPr-Ser46-P)–*ackA2* and CcpA–(HPr-Ser46-P)–*gntR-down* have 13, 13 and 14 side chain–base interactions, respectively (Figure 5C). While the *gntR-down* bound structure has more overall protein–DNA contacts, some of these contacts may be slightly unfavourable as they involve interactions between polar groups and hydrophobic groups, such as the Ala18-Cβ to Ade4 N6 interaction in one-half site and Ala18-Cβ to Gua13 O6 contact in the other half site. This contrasts with the non-polar or van der Waals contacts made by the Ala18 Cβ to thymine methyl groups observed in the syn and *ackA2* structures. Thus, the non-polar residues in the CcpA DNA-binding domain contribute to binding affinity whilst allowing promiscuity in nucleobase interactions. Of course, another factor contributing to binding strength but not specificity are the numerous side chain–phosphate backbone interactions. There are 24 such contacts in each complex.

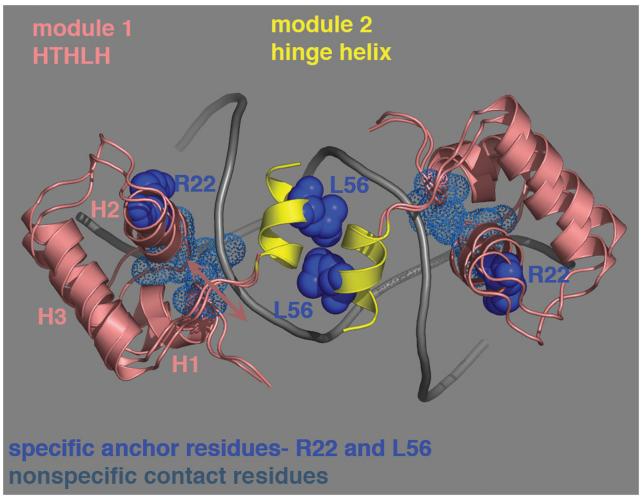

Figure 6. Key properties that allow CcpA to function as a global regulator. The DNA-binding properties of CcpA that are key for its global function include the utilization of two separable DNA-binding modules, the HTHLH motifs, which contacts the major groove, and the hinge helices, which contact the minor groove. The flexible linkage between the modules and an abundance of non-polar residues residing on the 'recognition helix' (α2), allow multiple, relatively non-specific nucleobase contacts and permit plasticity in both binding conformation and nucleobase recognition. The HTHLH (module 1) is shown as a pink ribbon whilst the hinge helix (module 2) is shown as a yellow ribbon. The flexible attachment of the HTHLH is indicated by an arrow and the extent of the flexibility is indicated by the overlays of the syn bound and the *ackA2* bound structures, which show the largest deviations. The *gntR–down* complex has a HTHLH position that is in between these two extremes. Residues that are involved in the recognition of the conserved G–C base pair (residue R22) and the central CpG step (residue L56) are shown as solid blue spheres. The residues of the recognition helix that make van der Waals contacts to the *cre* sites and allow DNA sequence promiscuity are shown as dotted cyan surfaces. The DNA sugar phosphate backbone is shown as a grey tube.

Like CcpA a number of bacterial transcription regulators function as global effectors of transcription by binding cognate DNA sites in the promoters of the genes they regulate. For example, the cAMP receptor protein (CRP), also known as CAP, functions analogously to the Gram-positive CcpA as the master regulator of carbon catabolite control in Gram-negative bacteria. CRP is activated to bind to its cognate 22-bp DNA site by first binding cAMP (49). Interestingly, unlike Gram-negative bacteria, Gram-positive bacteria do not normally contain cAMP, except under conditions of oxygen limitation. Thus, different mechanisms for CCR are clearly at play in Gram-negative compared to Gram-positive bacteria. Unlike CcpA, CRP, which regulates more than 200 genes, appears to bind its DNA sites with higher stringency, as 14 out of the 22 bp are recognized specifically (49). However, it remains to be seen whether CRP also displays some level of promiscuity in DNA binding. It would seem likely that all global transcription regulators would benefit from displaying some degree of plasticity in their DNA-binding capabilities. Further studies combining structural and biochemical analyses will be needed to address this important issue.

In summary, our structures of CcpA–(HPr-Ser46-P) bound to three divergent *cre* sites reveal two key features that help to explain how CcpA can bind *cre* sites with different DNA sequences but with similar affinities. First, the structures demonstrate that CcpA binds DNA using two flexibly attached DNA-binding modules: the HTHLH module and the hinge helix. The flexible linkage of the two modules permits them to dock favourably onto diverse DNA conformations, with conserved contacts between Arg22 and Gua3 primarily stabilizing the three helix bundle module onto the major grooves of each half site and the Leu56-CpG contacts locking the hinge helices into the DNA minor groove (Figure 6). Outside these G–C nucleotides, the other bases of the >50 *cre* sites show little conservation. This diversity is accommodated by the presence of a number of non-polar residues in the DNA-binding modules, particularly the HTH that can make numerous contacts that impart binding affinity without enforcing rigid specificity. In this way, CcpA can bind multiple sequences in the *B. subtilis* genome and function as a global regulator of transcription.

ACCESSION NUMBERS

Coordinates and structure factor amplitudes for the CcpA–(HPr-Ser46-P)–syn, CcpA–(HPr-Ser46-P)–*ackA2* and CcpA–(HPr-Ser46-P)–*gntR-down* structures have been deposited with the Protein Data Bank under the accession codes 3OQO, 3OQM and 3OQN, respectively.

SUPPLEMENTARY DATA

Supplementary Data are available at NAR Online.

ACKNOWLEDGEMENTS

We thank the Advanced Light Source (ALS) and their support staff. The ALS is supported by the Director, Office of Science, Office of Basic Energy Sciences and Material Science Division of the US Department of Energy at the Lawrence Berkeley National Laboratory. We also thank Gerald Seidel for constructing pWH653.

FUNDING

Funding for open access charge: MD Anderson Trust Fellowship; Burroughs Wellcome Career Development Award; National Institutes of Health (GM074815 to M.A.S.); Welch Foundation (G-0040 to R.G.B.); BMBF, BaCell-SysMO and Deutsche Forschungsgemeinschaft (SFB 476 to W.H.); Fonds der Chemischen Industrie (to W.H.).

Conflict of interest statement. None declared.

REFERENCES

1. Bruckner,R. and Titgemeyer,F. (2002) Carbon catabolite repression in bacteria: choice of the carbon source and autoregulatory limitation of sugar utilization. *FEMS Microbiol. Lett.*, **209**, 141–148.
2. Stülke,J. and Hillen,W. (1998) Coupling physiology and gene regulation in bacteria: the phosphotransferase sugar uptake system delivers the signals. *Naturwissenschaften*, **85**, 583–592.
3. Stülke,J. and Hillen,W. (2000) Regulation of carbon catabolism in *Bacillus* species. *Annu. Rev. Microbiol.*, **54**, 849–880.
4. Fujita,Y. (2009) Carbon catabolite control and the metabolic network in *Bacillus subtilis*. *Biosci. Biotechnol. Biochem.*, **73**, 245–259.
5. Deutscher,J. (2008) The mechanisms of carbon catabolite repression in bacteria. *Curr. Opin. Microbiol.*, **11**, 87–93.
6. Görke,B. and Stülke,J. (2008) Carbon catabolite repression in bacteria: many ways to make the most of nutrients. *Nat. Rev. Microbiol.*, **6**, 613–624.
7. Warner,J.B. and Lolkema,J.S. (2003) CcpA-dependent carbon catabolite repression in bacteria. *Microbiol. Mol. Biol. Rev.*, **67**, 475–490.
8. Weickert,M.J. and Adhya,S. (1992) A family of bacterial regulators homologous to Gal and Lac repressors. *J. Biol. Chem.*, **267**, 15869–15874.
9. Schumacher,M.A., Choi,K.Y., Zalkin,H. and Brennan,R.G. (1994) Crystal structure of LacI member, PurR, bound to DNA: minor groove binding by alpha helices. *Science*, **266**, 763–770.
10. Schumacher,M.A., Choi,K.Y., Lu,F., Zalkin,H. and Brennan,R.G. (1995) Mechanism of corepressor-mediated specific DNA binding by the purine repressor. *Cell*, **83**, 147–155.
11. Schumacher,M.A., Allen,G.S., Diel,M., Seidel,G., Hillen,W. and Brennan,R.G. (2004) Structural basis for allosteric control of the transcription regulator CcpA by the phosphoprotein HPr-Ser46-P. *Cell*, **118**, 731–741.
12. Bell,C.E. and Lewis,M. (2000) A closer view of the conformation of the Lac repressor bound to operator. *Nat. Struct. Biol.*, **7**, 209–214.
13. Bell,C.E. and Lewis,M. (2001) Crystallographic analysis of Lac repressor bound to natural operator *O1*. *J. Mol. Biol.*, **312**, 921–926.
14. Lewis,M., Chang,G., Horton,N.C., Kercher,M.A., Pace,H.C., Schumacher,M.A., Brennan,R.G. and Lu,P. (1996) Crystal structure of the lactose operon repressor and its complexes with DNA and inducer. *Science*, **271**, 1247–1254.
15. Deutscher,J., Küster,E., Bergstedt,U., Charrier,V. and Hillen,W. (1995) Protein kinase-dependent HPr/CcpA interaction links glycolytic activity to carbon catabolite repression in gram-positive bacteria. *Mol. Microbiol.*, **15**, 1049–1053.
16. Henkin,T.M. (1996) The role of the CcpA transcriptional regulator in carbon catabolite metabolism in *Bacillus subtilis*. *FEMS Microbiol. Lett.*, **135**, 9–15.
17. Aung-Hilbrich,L.M., Seidel,G., Wagner,A. and Hillen,W. (2002) Quantification of the influence of HPrSer46P on CcpA-*cre* interaction. *J. Mol. Biol.*, **319**, 77–85.
18. Jones,B.E., Dossonnet,V., Küster,E., Hillen,W., Deutscher,J. and Klevit,R.E. (1997) Binding of the catabolite repressor protein CcpA to its DNA target is regulated by phosphorylation of its corepressor HPr. *J. Biol. Chem.*, **272**, 26530–26535.
19. Galinier,A., Deutscher,J. and Martin-Verstraete,I. (1999) Phosphorylation of either Crh or HPr mediates binding of CcpA to the *Bacillus subtilis xyn cre* and catabolite repression of the *xyn* operon. *J. Mol. Biol.*, **286**, 307–314.
20. Audette,G.F., Engelmann,R., Hengstenberg,W., Deutscher,J., Hayakama,K., Quail,J.W. and Delbaere,L.T. (2000) The 1.9 Å resolution structure of phospho-serine 46 HPr from *Enterococcus faecalis*. *J. Mol. Biol.*, **303**, 545–553.
21. Moreno,M.S., Schneider,B.L., Maile,R.R., Weyler,W. and Saier,M.H. Jr (2001) Catabolite repression mediated by the CcpA protein in *Bacillus subtilis*: novel modes of regulation revealed by whole-genome analyses. *Mol. Microbiol.*, **39**, 1366–1381.
22. Turinsky,A.J., Grundy,F.J., Kim,J.H., Chambliss,G.H. and Henkin,T.M. (1998) Transcriptional activation of the *Bacillus subtilis ackA* gene requires sequences upstream of the promoter. *J. Bacteriol.*, **180**, 5961–5967.
23. Moir-Blais,T.R., Grundy,F.J. and Henkin,T.M. (2001) Transcriptional activation of the *Bacillus subtilis ackA*

promoter requires sequences upstream of the CcpA binding site. *J. Bacteriol.*, **183**, 2389–2393.
24. Pesecan-Siedel,E., Galinier,Z., Longin,R., Deutscher,J., Danchin,A., Glaser,P. and Martin-Verstraete,I. (1999) Catabolite regulation of the *pta* gene as part of carbon flow pathways in *Bacillus subtilis*. *J. Bacteriol.*, **181**, 6889–6897.
25. Shin,B.S., Choi,S.K. and Park,S.H. (1999) Regulation of the *Bacillus subtilis* phosphotransacetylase gene. *J. Biochem.*, **126**, 333–339.
26. Nicholson,W.L., Park,Y.K., Henkin,T.M., Won,M., Weickert,M.J., Gaskell,J.A. and Chambliss,G.H. (1987) Catabolite repression-resistant mutations of the *Bacillus subtilis alpha*-amylase promoter affect transcription levels and are in an operator-like sequence. *J. Mol. Biol.*, **198**, 609–618.
27. Krüger,S., Gerz,S. and Hecker,M. (1996) Transcriptional analysis of *bglPH* expression in *Bacillus subtilis*: evidence for two distinct pathways mediating carbon catabolite repression. *J. Bacteriol.*, **177**, 5590–5597.
28. Monedero,V., Boel,G. and Deutscher,J. (2001) Catabolite regulation of the cytochrome *c550*-encoding *Bacillus subtilis cccA* gene. *J. Mol. Microbiol. Biotechnol.*, **3**, 433–438.
29. Asai,K., Baik,S.H., Kasahara,Y., Moriya,S. and Ogasawara,N. (2000) Regulation of the transport system for C4-dicarboxylic acids in *Bacillus subtilis*. *Microbiology*, **146**, 263–271.
30. Darbon,E., Servant,P., Poncet,S. and Deutscher,J. (2002) Antitermination by GlpP, catabolite repression via CCpA and inducer exclusion triggered by P-GlpK dephosphorylation control *Bacillus subtilis glpFK* expression. *Mol. Microbiol.*, **43**, 1039–1052.
31. Grundy,F.J., Waters,D.A., Allen,S.H.G. and Henkin,T.M. (1993) Regulation of the *Bacillus subtilis* Acetate kinase gene by CcpA. *J. Bacteriol.*, **175**, 7348–7355.
32. Puri-Taneja,A., Paul,S., Chen,Y. and Hulett,F.M. (2006) CcpA causes repression of *phoPR* promoter through a novel transcription start site. *J. Bacteriol.*, **188**, 1266–1278.
33. Kim,J.H., Yang,Y.K. and Chambliss,G.H. (2005) Evidence that *Bacillus* catabolite control protein CcpA interacts with RNA polymerase to inhibit transcription. *Mol. Microbiol.*, **56**, 155–162.
34. Martin-Verstraete,I., Stulke,J., Klier,A. and Rapoport,G. (1995) Two different mechanisms mediate catabolite repression of the *Bacillus subtilis* levanase operon. *J. Bacteriol.*, **177**, 6919–6927.
35. Weickert,M.J. and Chambliss,G.H. (1989) Site-directed mutagenesis of a catabolite repression operator sequence in *Bacillus subtilis*. *Proc. Natl Acad. Sci. USA*, **87**, 6238–6242.
36. Miwa,Y., Nakata,A., Ogiwara,A., Yamamoto,M. and Fujita,Y. (2000) Evaluation and characterization of catabolite-responsive elements (*cre*) of *Bacillus subtilis*. *Nucleic Acids Res.*, **28**, 1206–1210.
37. Seidel,G., Diel,M., Fuchsbauer,N. and Willen,W. (2005) Quantitative interdependence of coeffectors, CcpA and *cre* in carbon catabolite regulation of *Bacillus subtilis*. *FEBS J.*, **272**, 2566–2577.
38. Lundblad,J.R., Laurance,M. and Goodman,R.H. (1996) Fluorescence polarization analysis of protein-DNA and protein-protein interactions. *Mol. Endocrinol.*, **10**, 607–612.
39. Horstmann,N., Seidel,G., Aung-Hilbrich,L.M. and Hillen,W. (2007) Residues His-15 and Arg-17 of HPr participate differently in catabolite signal processing via CcpA. *J. Biol. Chem.*, **282**, 1175–1182.
40. Chaptal,V., Guegen-Chaignon,V., Poncet,S., Lecampion,C., Meyer,P., Deutscher,J., Galingier,A., Nessler,S. and Morera,S. (2006) Structural analysis of *B.* subtilis CcpA effector binding site. *Proteins*, **64**, 814–816.
41. Brünger,A.T., Adams,P.D., Clore,G.M., DeLano,W.L., Gros,P., Crosse-Kunstleve,R.W., Jiang,J.S., Kuszewski,J., Nilges,M., Pannu,N.S. *et al.* (1998) Crystallography and NMR System: A new software suite for macromolecular structure determination. *Acta Crystallogr. D Biol. Crystallogr.*, **54**, 905–921.
42. Jones,T.A., Zou,J.-Y., Cowan,S.W. and Kjeldgaard,M. (1991) Improved methods for building protein models in electron density maps and the location of errors in these models. *Acta. Crystallogr.*, **A47**, 110–119.
43. Miwa,Y., Nagura,K., Eguchi,S., Fukuda,H., Deutscher,J. and Fujita,Y. (1997) Catabolite repression of the *Bacillus subtilis gnt* operon exerted by two catabolite-responsive elements. *Mol. Microbiol.*, **23**, 1203–1213.
44. Lavery,R., Moaker,M., Maddocks,J.H., Petkeviciute,D. and Zakrzewska,K. (2009) Conformational analysis of nucleic acids revisited: Curves+. *Nucleic Acids Res.*, **37**, 5917–5929.
45. Peters,J.P. 3rd and Maher,L.J. (2010) DNA curvature and flexibility *in vitro* and *in vivo*. *Rev. Biophys.*, **43**, 23–63.
46. Lamoureux,J.S., Stuart,D., Tsang,R., Wu,C. and Glover,J.N.M. (2002) Structure of the sporulation-specific transcription factor Ndt80 bound to DNA. *EMBO J.*, **21**, 5721–5732.
47. Lamoureux,J.S., Maynes,J.T. and Glover,J.N.M. (2004) Recognition of 5′-YpG-3′ sequences by coupled stacking/hydrogen bonding interactions with amino acid residues. *J. Mol. Biol.*, **335**, 399–408.
48. Olson,W.K., Gorin,A.A., Lu,X.J., Hock,L.M. and Zhurkin,V.B. (1998) DNA sequence-dependent deformability deduced from protein-DNA crystal complexes. *Proc. Natl Acad. Sci. USA*, **95**, 11163–11168.
49. Lawson,C.L., Swigon,D., Murakami,K.S., Darst,S.A., Berman,H.M. and Ebright,R.H. (2004) Catabolite activator protein (CAP): DNA binding and transcription activation. *Curr. Opin. Struct. Biol.*, **14**, 10–20.
50. Yoshida,K., Aoyama,D., Ishio,I., Shibayama,T. and Fujita,Y. (1997) Organization and transcription of the *myo*-inositol operon, *io1*, of *Bacillus subtilis*. *J. Bacteriol.*, **179**, 4591–4598.
51. Miwa,Y. and Fujita,Y. (2001) Involvement of two distinct catabolite-responsive elements in catabolite repression of the *Bacillus subtilis myo*-inositol (*io1*) operon. *J. Bacteriol.*, **183**, 5877–5884.
52. Yoshida,K., Ishio,I., Nagakawa,E., Yamamoto,Y., Yamamoto,M. and Fujita,Y. (2000) Systematic study of gene expression and transcription organization in the *gntZ-ywaA* region of *Bacillus subtilis* genome. *Microbiology*, **146**, 573–579.
53. Choi,S.K. and Saier,M.H. Jr (2005) Regulation of *sigL* expression by the catabolite control protein CcpA involves a roadblock mechanism in *Bacillus subtilis*: potential connection between carbon and nitrogen metabolism. *J. Bacteriol.*, **187**, 6856–6861.
54. Yamamoto,H., Murata,M. and Sekiguchi,J. (2000) The CitST two-component system regulates the expression of the Mg-citrate transporter in *Bacillus subtilis*. *Mol. Microbiol.*, **37**, 898–912.
55. Delano,W.L. (2002) *The PyMOL Molecular Graphics System*. DeLano Scientific, San Carlos, California.
56. Parche,S., Schmid,R. and Titgemeyer,F. (1999) The phosphotransferase system (PTS) of *Streptomyces coelicolor* identification and biochemical analysis of a histidine phosphocarrier protein HPr encoded by the gene *ptsH*. *Eur. J. Biochem.*, **265**, 308–317.
57. Reizer,J., Hoischen,C., Titgemeyer,F., Rivolta,C., Rabus,R., Stülke,J., Karamata,D., Saier,M.H. Jr and Hillen,W. (1998) A novel protein kinase that controls carbon catabolite repression in bacteria. *Mol. Microbiol.*, **27**, 1157–1169.